BMP-dependent oligoclonal cancer attractor state precedes neural crest fate in melanoma initiation

Alicia M. McConnell[1,2,3,#], Maggie H. Chassé[1,2,3,#], Haley R. Noonan[1,2,3,4], Jeffrey K. Mito[1,2,3,5], Julia Barbano[1], Erika Weiskopf[1], Irene F. Gosselink[1], Song Yang[1,2,3], Kyle D. Drake[1,2,3], Chloé S. Baron[1,2,3], Elise Layne[1,2,3], Meera Prasad[1,2,3], Phammela Abarzua[6], Maxime Grimont[7], Yung-Ching Kao[8], Christine G. Lian[6], Anaïs Eberhardt[7,9], Marie Donzel[10], Katie J. Lee[8], Iwei Yeh[11], George F. Murphy[6], Mitchell S. Stark[8], Stéphane Dalle[7,9], Julie Caramel[7], Cole Trapnell[12], and Leonard I. Zon[1,2,3*]

[1] Stem Cell and Regenerative Biology Program and Division of Hematology/Oncology, Children's Hospital Boston, Howard Hughes Medical Institute, Boston, MA 02115, USA.

[2] Harvard Stem Cell Institute, Boston, MA 02115, USA.

[3] Harvard Medical School, Boston, MA 02115, USA.

[4] Biological and Biomedical Sciences Program, Harvard Medical School, Boston, Massachusetts 02115, USA.

[5] Department of Pathology, Brigham and Women's Hospital, Boston, MA 02215, USA.

[6] Program in Dermatopathology, Department of Pathology, Brigham and Women's Hospital, Boston, MA 02215, USA.

[7] Centre de Recherche en Cancérologie de Lyon, INSERM U1052-CNRS UMR5286, Centre Léon Bérard, Université de Lyon, Université Claude Bernard Lyon1, 69008, Lyon, France.

[8] Frazer Institute, The University of Queensland, Dermatology Research Centre, Brisbane, Australia.

[9] Dermatology Department, Hospices Civils de Lyon, Centre Hospitalier Lyon Sud, Pierre Bénite, France.

26 [10] Pathology Department, Hospices Civils de Lyon, Centre Hospitalier Lyon Sud, Pierre Bénite,
27 France.
28 [11] Department of Dermatology & Pathology, University of California San Francisco, San
29 Francisco CA 94115, USA.
30 [12] Department of Genome Sciences, University of Washington, Seattle, WA, 98195, USA.
31 # These authors contributed equally.
32 * Corresponding author: zon@enders.tch.harvard.edu
33

Field cancerization posits that groups of cells harboring oncogenic mutations create a permissive landscape predisposed to malignant transformation. We previously identified rare single cells in BRAF^{V600E};p53$^{-/-}$ zebrafish that reactivate an embryonic neural crest program prior to melanoma initiation. Here, we identify a specific field of BRAF^{V600E};p53$^{-/-}$ melanocytes with altered differentiation, morphology and cell-cycle regulatory programs that predates the neural crest activation. Based on single cell analysis, these cells form a cancer precursor zone (CPZ) from which a single clone ultimately stabilizes a neural crest–like state and expands to form melanoma. Using in vivo cellular barcoding combined with single-cell RNA-seq and ATAC-seq, we identify a transcriptionally distinct attractor state specific to oligoclonal CPZs that is modulated by BMP signaling. Mechanistically, BMP-dependent induction of the transcriptional repressor ID1 sequesters TCF12, thereby inhibiting lineage-specific targets required for maintenance of melanocyte identity and for clonal selection. Single cells from the CPZ initiate neural crest reprogramming and become tumorigenic. Analysis of a large human patient cohort reveals high ID1 expression in precursor melanocytes as early as dysplastic nevi and atypical melanocytic proliferations, implicating ID1 in early human melanomagenesis. This work identifies BMP signaling and ID1 as early, targetable vulnerabilities with potential for improved diagnosis and prevention of melanoma. Together, these findings uncover a previously unrecognized field effect during melanoma initiation, in which tumors emerge from an oligoclonal attractor-state zone of morphologically distinct yet clinically covert precursor cells with a defined altered transcriptional fate.

Melanoma incidence has increased dramatically over the past three decades, yet the earliest stages of melanomagenesis remain poorly defined. Multiple studies report substantial variability among pathologists in the diagnosis of early precursor lesions, underscoring a fundamental gap in our understanding of melanoma initiation(*1-4*). Over 80% of melanomas

59 harbor activating MAPK pathway mutations, most commonly *BRAF*^{V600E}, frequently
60 accompanied by tumor suppressor loss-of-function mutations(*5, 6*). However, *BRAF*^{V600E} alone
61 is insufficient to drive melanoma**,** as 82–100% of benign nevi carry this mutation yet never
62 progress(*7, 8*). Further, subclinical fields of *BRAF*^{V600E} are prevalent in human skin, with
63 enrichment near prior melanoma excisions and benign nevi(*9*). These observations suggest that
64 many potential melanoma precursors remain clinically covert and molecularly undefined.
65 To investigate the earliest determinants of melanoma initiation, we developed a
66 zebrafish model in which p53$^{-/-}$ melanocytes express BRAF^{V600E}. Despite the presence of a
67 widespread cancerized melanocyte field, individual fish develop only 1-3 tumors, with minimal
68 additional mutational burden(*10, 11*). This constrained tumor output mirrors human disease and
69 implies the existence of rate-limiting, non-genetic barriers to malignant
70 transformation. Understanding how genetically primed melanocytes clonally expand may
71 therefore be central to melanoma initiation, yet the clonal dynamics of melanomagenesis remain
72 largely unexplored, in contrast to other tumor types(*12-16*).

73 We previously demonstrated that individual BRAF^{V600E};p53$^{-/-}$ melanocytes undergo
74 neural crest reprogramming to initiate melanoma(*11, 17*). Here, we identify oligoclonal cancer
75 precursor zones (CPZs), a previously unrecognized intermediate state composed of
76 morphologically and transcriptionally aberrant melanocytes. Time-course imaging shows that
77 CPZ formation is necessary for tumor initiation, marking a key transition in melanoma
78 progression. CPZ melanocytes upregulate BMP signaling, and cellular barcoding studies
79 indicate oligo clonal expansion and subsequent clonal dominance and progression toward
80 monoclonal tumors. This process depends on ID1-mediated sequestration of TCF12, which
81 represses differentiation programs and stabilizes a precursor attractor state. Together, our data
82 position CPZs as a critical bottleneck in melanoma initiation and provide a mechanistic

83 framework for how permissive melanocytes transform and reinforce neural crest–like programs
84 to drive melanoma.

85 **Melanoma forms in oligoclonal cancer precursor zones**

86 To characterize the earliest stages of melanoma formation, we generated *p53* deficient,
87 *crestin:EGFP* zebrafish in which melanocytes express $BRAF^{V600E}$, are marked red by
88 *mitfa:mCherry,* and are amelanotic (referred to as *BRAF;p53*)(*11, 18, 19*). We performed time
89 course imaging and found that prior to neural crest reactivation, there were regions of hundreds
90 of morphologically aberrant melanocytes expressing high levels of *mitfa:mCherry*, which we term
91 the cancer precursor zone (CPZ; Fig. 1A, Supp. Fig. 1A-C). We followed a cohort of fish that
92 exhibit varying kinetics of CPZ formation and neural crest reactivation with an average onset of
93 11- and 15-weeks post-fertilization (wpf), respectively (Fig. 1B, Supp. Fig. 1D). While on average
94 only 70% of CPZs reactivate *crestin:EGFP* to form a tumor, individual neural crest reactivated
95 *crestin*+ cells within the CPZ inevitably go on to form a melanoma and crestin+ cells do not arise
96 from non-CPZ sites (Fig. 1A,B; Supp. Fig 1B,C). We correlated our imaging with histological
97 analysis of mitfa and crestin across initiation stages, confirming that individual *crestin* positive
98 cells give rise to tumors (Fig. 1C). Further, CPZs form in two additional zebrafish melanoma
99 models (*mcr:BRAF*^{V600E} and *mcr:NRAS*^{Q61R}) without p53 inactivation, suggesting cancer precursor
100 zones are not specific to $BRAF^{V600E}$ and are not dependent on p53 loss (Supp. Fig. 1E,F).
101

102 **Cancer precursor zones are oligoclonal and have aberrant morphology**

103 In line with previous studies, CPZs arise across the entire fish body with more frequent
104 localizations in the head, dorsal fin, and tail base(*20*) with a range of sizes ($0.54\pm0.27mm^2$) and
105 *mitfa:mCherry* intensities (105.6±27.4 a.u.) (Supp. Fig. 2A-C). Despite the presence of oncogenic
106 mutations, the cancerized field melanocytes appear morphologically normal, with proper dendrite
107 formation and spacing throughout the skin (Supp. Fig. 3A, left). However, upon CPZ formation,

108 the melanocytes exhibit aberrant morphology with loss of dendrites (Supp. Fig. 3A, right). Further,
109 histological analysis shows that CPZ melanocytes encompassing *crestin:EGFP*+ cells are highly
110 proliferative with large nuclei (Supp. Fig. 3B,C). Our zebrafish model reveals a novel intermediate
111 step between cancerized field melanocytes and tumor initiation, where morphologically abnormal
112 cancer precursor zone melanocytes encompass the cell undergoing neural crest progenitor state
113 activation as it transforms.

114 To understand how melanoma clonally evolves, we utilized GESTALT, an in vivo CRISPR-
115 Cas9 based lineage tracing approach, in its first application of melanoma initiation and solid tumor
116 evolution(*21, 22*). We induced two rounds of sgRNA-directed barcoding of the GESTALT cassette
117 at the single cell stage and at 48 hpf, corresponding to the birth of the adult melanocyte stem
118 cell(*23*). We sorted *mitfa:mCherry*+ melanocytes from each melanoma stage and analyzed clone
119 number following DNA sequencing of the GESTALT cassette (Supp. Fig. 4A-D). Healthy
120 melanocytes (29.8±4.9 clones) and cancerized field melanocytes (18.9±4.2 clones) are polyclonal
121 with no evidence of clonal dominance, as indicated by a lack of clones reaching greater than 20%
122 of total reads (three S.D. higher than the average cancerized field clone). CPZ formation is
123 oligoclonal compared to normal skin melanocytes (5.3±1.3 clones) while tumors form from 1-2
124 clones (1.8±0.5 clones) (Fig. 1D). This marked decrease in clone number was accompanied by a
125 significant increase in the size of the dominant clone (Fig. 1E). Further, the decreased Shannon
126 entropy with a corresponding increase in Gini coefficient and leftward shift in the Lorenz curves
127 as melanoma progresses highlights a decline in clonal diversity in CPZs and the subsequent
128 emergence of a dominant malignant clone (Fig. 1F, Supp. Fig. 4F-J). Together these data indicate
129 melanoma arises through a stepwise clonal bottleneck, with polyclonal melanocytes developing
130 into to oligoclonal CPZs and ultimately a single dominant tumor clone.

131 To determine if CPZs have malignant potential, we FACS isolated melanocytes from
132 normal skin, the cancerized field, and cancer precursor zones, as well as small *crestin*+ patches,
133 or tumors for transplantation (Supp. Fig. 5A). Cells injected under the skin of irradiated recipient

134 fish and a limit dilution assay was performed at 14 days post-transplant. CPZ cells engrafted at
135 about half the rate (0.43x) of *crestin*+ cells from small patches or tumors, while normal or
136 cancerized field melanocytes did not engraft (Fig. 1G, Supp. Fig. 5B). Small *crestin* patch cells
137 engrafted at a similar rate to tumor cells, suggesting that neural crest reactivated cells have similar
138 malignant potential. Together, these data demonstrate a substantial clonal selection from the
139 cancerized field melanocytes, providing a set of cells that gain malignant potential and could
140 become tumorigenic. Further clonal restriction occurs from the pool of CPZ clones to form
141 monoclonal tumors.
142
143 **Cancer precursor zones are transitory with distinct transcriptional and chromatin states**
144 *BRAF;p53* zebrafish only develop one to three melanomas over their lifetime with minimal
145 additional genetic mutations(*10*), indicating that transcriptional changes are key drivers of
146 melanoma initiation. To explore this, we performed single-cell RNA-seq (scRNA-seq). Control
147 cancerized field, cancer precursor zones, or small *crestin* patches were isolated and run through
148 the 10X Genomics scRNA-seq platform (Fig 2A, Supp. Fig. 6A,B). scRNA-seq module scores
149 for mitfa+/mCherry+ cells were elevated in both CPZ and crestin+ patch populations,
150 whereas crestin+/EGFP+ module scores were high only in crestin+ patch cells, consistent with
151 the dynamics observed in time-course imaging (Fig. 1A, Fig. 2B,C). Dimensional analysis
152 highlights cellular reprogramming from cancerized field melanocytes to crestin+ melanoma with
153 CPZ melanocytes as a transitory population, with an independent analysis using InDrop scRNA-
154 seq showing similar results (Fig. 2D-I, Supp. Fig. 6C-H). CPZ cells express both melanoblast
155 (e.g., *tfap2a*, *tfap2e, runx3)* and neural crest markers (e.g., *foxd3* and *sox10*) highlighting the
156 transitory transcriptome of this population (Fig. 2J). These analyses reveal that the transformation
157 of a terminally differentiated melanocyte occurs through a transcriptional shift through a cancer
158 precursor zone and towards a neural crest progenitor state.

159 To verify CPZ cells are a transitory population in melanoma initiation, we performed RNA-
160 seq on FACS isolated *mitfa:mCherry*+ cancerized field melanocytes and compared them to
161 *mitfa:mCherry*+ CPZ melanocytes and *mitfa:mCherry+/crestin:EGFP*+ cells isolated from small,
162 medium, and large *crestin* patches. CPZ induction did not cause a global impact on gene
163 expression relative to cancerized field with only 502 genes (2.8% [n=17,483], $\log_2$FC±2, p-value
164 <0.001) altering in expression, indicating this transcriptional switch is specific to progression in
165 melanomagenesis (Supp. Fig. 7A-C).Due to these changes in gene expression, PCA analysis
166 shows that the sorted melanocytes cluster according to stage, with the cancer precursor zone
167 melanocytes overlapping both the cancerized field and *crestin* patch clusters (Supp. Fig. 7D). This
168 suggests that the cancer precursor zone cells represent a transition state between the cancerized
169 field and neural crest reactivated cells.

170 The distinct gene expression signatures separating melanocytes, cancer precursor zones,
171 and *crestin* positive cells indicates that melanoma initiation occurs through unique transcriptional
172 cell states. Differential expression analysis of both the scRNA-seq and RNA-seq data revealed
173 stage-specific expression signatures (Fig. 2J, Supp. Fig. 8A). CPZ cells have increased
174 expression of BMP signaling (red), as well as neural plate border and pre-migratory neural crest
175 transcription factors (green). These expression profiles were correlated with gene expression at
176 various stages of human melanoma formation from two published datasets (Supp. Fig. 8B,C)(*24,*
177 *25*). Together, these findings support a conserved, stage-specific transcriptional trajectory in
178 which melanoma initiation arises from a distinct cellular state that mirrors programs observed
179 during human melanomagenesis.

180 To dissect the chromatin landscape, we performed ATAC-seq on sorted melanocytes from
181 various stages of initiation. We filtered called peaks for direct overlap or within a 5000 bp distance
182 of annotated genes for differential accessibility analysis (multiple tests corrected with FDR <0.05).
183 Only 999 genes (2.8% [n=35,592 total], $\log_2$FC±2.0, p-value <0.001) had differentially accessible

184 regions (DAR) in cancer precursor zone melanocytes relative to cancerized field (Supp. Fig. 9A-
185 C). Promoter and enhancer regions associated with differentially expressed genes contained
186 peaks that opened in a stage-specific manner (Fig. 2K, Supp. Fig. 10). Like RNA-seq, ATAC-seq
187 showed reprogramming of specific loci. and further indicate that a transcriptionally driven cancer
188 attractor state is present at the earliest stages of melanoma initiation.
189
190 **Cancerized field lacks MAPK activation**
191 Most human melanomas arise de novo, with only a small fraction of nevi progressing to
192 malignancy(*26*). However, 82-100% of benign nevi carry the *BRAF*^{V600E} mutation and activation
193 of the MAPK pathway does not always directly correlate with *BRAF* mutations in many
194 melanomas(*7, 8, 26-29*). Despite the presence of constitutively active BRAF in our zebrafish
195 model, the expression levels of MAPK pathway members and downstream targets are
196 upregulated exclusively in cancer precursor zone and *crestin*+ cells (Supp. Fig. 11A). Negative
197 regulators of MAPK, *spry2*, *spry4*, *dusp2*, and *dusp6*, show little to no expression, with
198 corresponding closed chromatin in the cancerized field melanocytes (Supp. Fig. 11A, B).
199 Importantly, ATAC-seq analysis on isolated melanocytes revealed that the enhancer regions
200 around MAPK target genes are not open in cancerized field but become open in cancer precursor
201 zones (Supp Fig. 10B). Furthermore, phospho-ERK immunohistochemistry showed no staining in
202 cancerized field melanocytes, low staining in *mitfa*^{med} CPZs, and high staining in *mitfa*^{high} CPZs
203 (Supp. Fig. 11C). We considered the possibility that the *mitfa*^{high} state increases the amount of
204 BRAF^{V600E} expression due to the *mitfa:BRAF*^{V600E} transgene; however, RNA-seq on isolated
205 melanocytes shows no change in BRAF^{V600E} expression between the cancerized field and CPZ
206 stages, only increasing at the patch stage (Supp. Fig. 11D). Together these data indicate that the
207 MAPK pathway is not active until the cancer precursor zone stage and is further activated during
208 tumor initiation.
209

210 **ID1 identifies and drives precursor zone formation**

211 Given that cancer precursor zones form prior to, and have a distinct transcriptional state from
212 cancerized field or *crestin* patches, we hypothesized the CPZ state is independently regulated.
213 As CPZs had high expression of BMP pathway members and downstream targets (Fig. 2J), and
214 BMP signaling has an established role in neural crest development(*30-32*), we next interrogated
215 the role of BMP signaling in melanoma initiation. We first confirmed endogenous upregulation of
216 *ID1* in CPZs by RNAscope in situ hybridization(*33*). *ID1* is highly expressed in CPZ melanocytes
217 but not in adjacent cancerized field cells (Supp. Fig. 12). Next, we used the MiniCoopR system to
218 overexpress *ID1*, a constitutively active *SMAD1* (caSMAD), or a dominant negative *BMP* receptor
219 (dnBMPR) in melanocytes(*18*). Activation of BMP signaling (MCR:caSMAD) significantly
220 increased CPZ incidence and subsequent tumor onset, while inhibition of BMP signaling
221 (MCR:dnBMPR) reduced CPZ and tumor incidence (Fig. 3A-D). Taken together, these data
222 support a model in which BMP signaling regulates the emergence of CPZs, establishing a critical
223 early step in melanoma initiation.

224 We next hypothesized BMP activity modulates clonal expansion in melanomagenesis.
225 Indeed, activation of BMP signaling (MCR:caSMAD) decreased CPZ clone number (MCR:MCS:
226 5.6±1.6; MCR:ID1: 3.6±0.9; MCR:caSMAD: 2.4±0.9 clones) and Shannon entropy while driving
227 clonal expansion, leading to a shift in the Lorenz curve, without significantly altering the Gini
228 coefficient relative to control as measured by GESTALT cellular barcoding (Fig. 3E-F, Supp. Fig.
229 13). Conversely, BMP inhibition (MCR:dnBMPR) increased CPZ clone number (17.3±3.4 clones)
230 and Shannon entropy, reduced the dominant clone's size and lowered the Gini coefficient (Fig.
231 3E-F, Supp. Fig. 13). Together, these data indicate that BMP activation drives clonal consolidation
232 towards oligoclonality, whereas BMP inhibition promotes a more diverse polyclonal landscape.

233 While BMP is necessary for CPZ clonal expansion, ID1 overexpression is not sufficient to
234 drive CPZ formation in the absence of $BRAF^{V600E}$ (Fig. 3H). Next, to highlight the role of MAPK
235 signaling in BMP activation, RNA-seq of human primary immortalized melanocytes (PMEL(*34*))

236 with and without BRAF^{V600E} (PMEL-BRAF) exhibited differential gene expression of known BMP
237 activators and responders highlighting the activation of BMP signaling following BRAF^{V600E}
238 overexpression, as we had observed in the zebrafish (Fig. 3I). Overall, these results provide
239 evidence that the stages of melanoma initiation are independently regulated with BMP signaling
240 driving CPZ initiation and not only clonal selection to tumorigenic cells. Perturbation of signaling
241 leads to a clonal selection and expansion, providing a pool of clones for subsequent tumor
242 formation.

243 To verify the role of ID1 in human melanoma, we performed immunofluorescence staining
244 on patient samples from four independent cohorts across various melanoma stages from healthy
245 skin to thick melanoma. The percent of melanocytes expressing ID1 and the intensity of ID1
246 staining was significantly increased in patient samples with atypical melanocyte proliferative
247 (potentially precursor) zones, melanoma in situ, or invasive melanoma compared to those in
248 normal skin (Fig. 4A-D, Supp. Fig. 14). In addition to more cells expressing ID1 as melanoma
249 initiates, cells also have higher ID1 expression (Fig. 4E). The ability of ID1 to initiate CPZs in the
250 zebrafish and the appearance of ID1 in atypical melanocytic hyperplasia fields validate the role
251 for ID1 in melanomagenesis and identify clinically covert ID1+ melanocytic precursor lesions in
252 humans.

253

254 **ID1 sequesters TCF12 from chromatin to drive initiation**

255 ID1 is overexpressed in over 20 types of cancer, including melanoma, where strong ID1
256 expression was significantly associated with increased tumor thickness and decreased patient
257 survival(*35, 36*). ID1 is a transcriptional repressor that prevents basic helix-loop-helix (bHLH)
258 transcription factors from binding to DNA(*37*). We performed IP-MS on A375 melanoma cells
259 overexpressing V5-tagged ID1 or Clover control. The bHLH factor TCF12 was the most
260 significantly pulled down protein with ID1 (Fig. 5A, Supp. Fig. 15A). When performing ATAC-seq
261 on sorted melanocytes isolated from ID1-overexpressing zebrafish, we found significant

262 enrichment of the TCF12 motif (ACAGCTG) under peaks that decreased with ID1 overexpression,
263 indicating ID1 is a repressor of TCF12 signaling (HOMER, p=1e-20). Predicted downstream
264 targets of TCF12 are significantly decreased in CPZs where ID1 is most highly expressed (Supp.
265 Fig. 15B)(*38*). Next, we performed RNA-seq on sorted melanocytes from zebrafish
266 overexpressing ID1 and identified potential downstream targets that were downregulated
267 following ID1-overexpression or in CPZs (Supp. Fig. 15C,D). TCF12 motifs were found under
268 open chromatin peaks in the promoter/enhancer regions associated with these genes, many of
269 which are important for dendritic processes and cell adhesion programs (e.g., *rhogb*, *parvg*,
270 *lamc1*, and *enah*) (Fig. 5B). Together, these results indicate that ID1 promotes melanoma
271 progression by repressing TCF12-mediated transcriptional programs critical for melanocyte
272 differentiation and cell proliferation.

273 To identify the repressed TCF12 genes, we next performed ChIP-seq following ID1 or
274 clover overexpression in PMEL-BRAF melanocytes. ID1 overexpression led to a marked
275 reduction in TCF12 chromatin occupancy and loss of TCF12 motif enrichment relative to control
276 (Fig. 5C,D). This marked decrease focally affected melanocyte development and neuronal genes,
277 including cell body, synapse regulation, and somatodendritic compartment regulation (Fig. 5E;
278 Supp. Fig. 15E). Specifically, ID1-OE led to loss of TCF12 occupancy at known neuronal genes,
279 and melanoma tumor suppressor genes, *DLGAP4* and *UNC5A*(*39-43*). In addition to known
280 markers of the neural lineage, TCF12 occupancy was lost at established melanin production
281 genes, such as *PKNOX2* and *PRKCZ*(*44*), (*45*), suggesting CPZs may represent unpigmented
282 precursor lesions. During CPZ formation, melanocytes attain an aberrant morphology, including
283 a loss of dendrites, which potentially achieved via a decrease in these targets.

284 To explore how modulation of the ID1/TCF12 axis alters cell viability, we measured
285 proliferation in PMEL-BRAF cells. ID1 overexpression led to a significant increase in cell
286 proliferation relative to control, likely due to the loss of development and cell cycle regulators (Fig.
287 5F). Conversely, TCF12 overexpression or siRNA knockdown of ID1 reduced cell viability.

288 Consistent with our findings in human cell lines, TCF12 overexpression in zebrafish using the
289 MiniCoopR system led to a significant decrease in the number of CPZs formed and tumor onset
290 compared to control (Fig. 5G,H). In both a zebrafish model and human immortalized melanocytes,
291 modulation of TCF12 expression reduces proliferation and oncogenic potential. In total, these
292 data support the hypothesis that ID1 binds to and inhibits TCF12, preventing it from activating
293 downstream targets thereby enabling morphological and transcriptional changes to form
294 oligoclonal cancer precursor zones, a novel initiating lesion in melanoma.
295

296 **Discussion**

297 Our studies identify a cancer precursor zone (CPZ) as a spatially restricted, oligoclonal
298 attractor state that precedes melanoma initiation. CPZs arise as contiguous fields of
299 melanocytes undergoing coordinated clonal expansion, displaying altered morphology and
300 distinct transcriptional profiles. These zones act as self-sustaining reservoirs of cells that
301 generate transcriptional diversity, enabling individual clones to independently explore alternative
302 cell-state trajectories. Rare, clone-restricted transitions within CPZs are marked by neural crest
303 fate reactivation, after which a single clone dominates and initiates tumor formation. Importantly,
304 these findings align with cell-of-origin studies showing transformation of interfollicular and
305 differentiated melanocytes in the mouse tail(*13*).

306 CPZs are stabilized by BMP–ID1–TCF12 signaling, which suppresses terminal
307 melanocyte differentiation and synchronizes transcriptional programs across neighboring cells,
308 maintaining cells within a shared, stable transcriptional attractor. This signaling axis balances
309 clonal fitness, enabling multiple clones to expand in parallel and persist as an oligoclonal
310 population over extended periods. These findings are consistent with a model in which BMP
311 signaling stabilizes adult stem and progenitor cells within a reversible “holding” state, preserving
312 future plasticity by restricting premature fate commitment(*46-51*). Subtle differences in BMP–ID1

signaling or downstream transcriptional rewiring allow rare clones to escape the CPZ attractor, enter neural crest–like transcriptional trajectories, and acquire tumor-initiating potential, paralleling clonal hematopoiesis[43] and providing a mechanistic explanation for both long-term oligoclonality and the low frequency of malignant progression.

Zebrafish CPZ melanocytes closely resemble atypical melanocytic proliferative lesions in early-stage human samples, highlighting cross-species conservation and revealing a potential window for preventative therapy. CPZs function as dynamic reservoirs where developmental and transcriptional programs guide cell behavior rather than immediate tumor formation. Many CPZs remain arrested despite ongoing clonal expansion, but rare clones stochastically activate neural crest progenitor-like programs and transition toward tumorigenesis. These findings suggest that early interventions targeting CPZ dynamics could suppress tumor initiation before malignant transformation occurs.

More broadly, our results support the cancer attractor state model, showing that tumor initiation is governed by entry into, maintenance of, and rare escape from a defined precursor state. Here, we show this precursor state is clonally derived from mature tissue populations. Oligoclonal precursor fields, like CPZs, have also been described in Barrett's esophagus, ductal carcinoma in situ, prostatic intraepithelial neoplasia, the uterine cervix, and familial adenomatous polyposis(*52-56*). Together, these observations indicate that malignancy often emerges from stable multicellular precursor states that channel evolutionary trajectories over time. By resolving CPZ dynamics in vivo, our work reframes melanoma initiation as a multistep process shaped by attractor stability and clone-specific escape events. This model highlight opportunities for early intervention by stabilizing precursor states or preventing escape, thereby providing a framework for cancer prevention strategies targeting transcriptional and epigenetic states.

337

338 **Author Contributions**

339 A.M.M., M.H.C., and L.I.Z. conceived of the study; L.I.Z. and G.F.M. supervised the research;
340 A.M.M. and M.H.C. designed and performed experiments with the assistance of H.R.N., J.B.,
341 E.W., I.F.G., E.L., K.D.D., C.S.B., and P.A.; J.K.M. assisted with histology and pathologic
342 assessment of fish and human samples; A.M.P., S.Y., C.L. performed computational analysis for
343 all sequencing experiments; C.G.L. A.E., M.D., M.S.S., S.D., J.C., I.W., provided human samples
344 and pathologic analysis. M.G., Y.K., K.J.L performed immunofluorescent staining and analysis on
345 human samples.

346

347 **Acknowledgements**

348 We would like to thank Christian Lawrence, Shane Hurley, Li-Kun Zhang, Kara Maloney, and
349 Hannah Nations for expert fish care. The authors thank many of their colleagues for their
350 discussions and critical reading of the manuscript. We thank Dana-Farber/Harvard Cancer Center
351 for the use of the Specialized Histopathology Core, which provided histology and
352 immunohistochemistry service. The authors would like to thank the Neurobiology Imaging Facility
353 (NIF) at Harvard Medical School for performing the RNAscope and the Single Cell Biology core
354 for assisting with the sequencing of the single cell atlas. We further acknowledge the assistance
355 the Translational Research Institute Microscopy Core Facility at the University of Queensland.
356 The Dana-Farber/Harvard Cancer Center is supported in part by an NCI Cancer Center Support
357 Grant #P30CA06516. We thank Ross Tomaino and the Harvard Medical School Taplin Mass
358 Spectrometry Facility for their assistance in performing and analyzing our mass spectrometry
359 experiments. This work was supported by R01CA103846-14, American Cancer Society
360 Postdoctoral Fellowship PF-18-150-01-DCC (A.M.M.), K00CA253749 (M.H.C.), and
361 F32CA294934 (K.D.D.). L.I.Z. is a Howard Hughes Medical Institute Investigator. This work was
362 also supported by Lyon Integrated Research Institute in Cancer (J.C., S.D.), Institut Convergence

389 **Figure 1 | Cancer precursor zone formation precedes neural crest reactivation in**
390 **zebrafish. A,** Melanoma initiation in zebrafish occurs in stages, beginning with the
391 formation of a cancerized field of rescued melanocytes, which expand to form a cancer
392 precursor zone. Neural crest reactivation occurs in cells within the cancer precursor
393 zone and tumor formation follows, with all tumor cells becoming *crestin:EGFP*+. Scale
394 bar: 1 mm. **B,** Swimmers plot of 13 zebrafish during melanoma initiation shows variable
395 onset of CPZ and neural reactivation (# represents fish time course in Fig. 1A; *
396 represents fish time course in Supp. Fig. 1C). **C**, Transverse sections of zebrafish skin
397 stained for mCherry and EGFP at the cancerized field, cancer precursor zone, neural
398 crest reactivation, and tumor formation stages. Scale bars, 100 μm. **D-F,** Violin plot of
399 the total clone number with a minimum clone size of 1.5% (**D**), the largest clone as
400 measured by the clone with the largest percent of total reads (**E**), and the Shannon
401 entropy (**F**) in a cohort of GESTALT barcoded fish (n=12 fish). *, $p \leq 0.05$; ****$p \leq 0.0001$.
402 **G**, Limit dilution curves at 14 days post-transplant (dpt). Confidence interval estimate is
403 displayed as 1/(engraftment cell frequency).
404
405
406
407
408
409
410

Figure 1

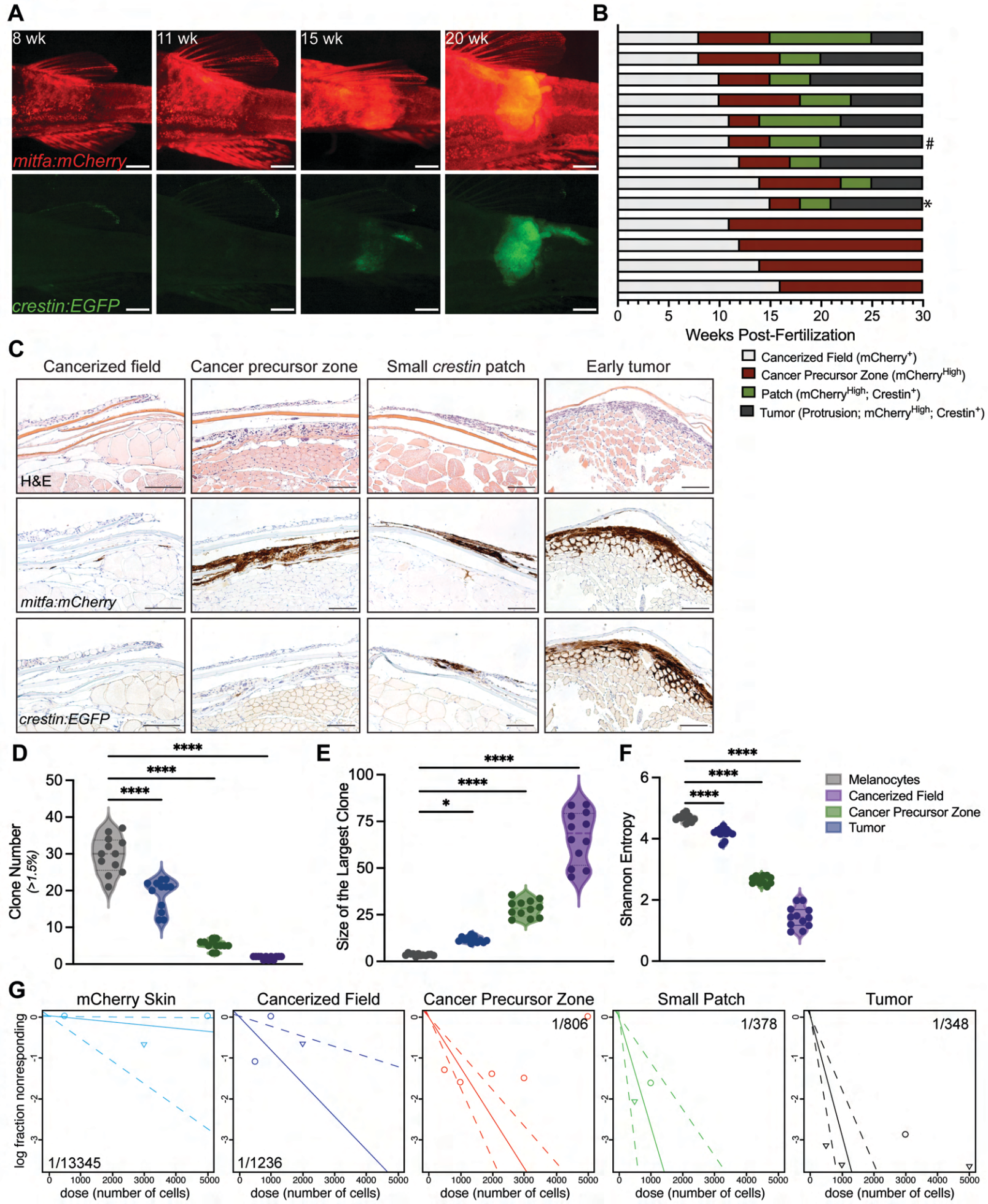
A
8 wk
11 wk
15 wk
20 wk
mitfa:mCherry
crestin:EGFP
B
#
*
0
5
10
15
20
25
30
Weeks Post-Fertilization
C
Cancerized field
Cancer precursor zone
Small crestin patch
Early tumor
H&E
mitfa:mCherry
crestin:EGFP
Cancerized Field (mCherry+)
Cancer Precursor Zone (mCherryHigh)
Patch (mCherryHigh; Crestin+)
Tumor (Protrusion; mCherryHigh; Crestin+)
D
Clone Number (>1.5%)
****
E
Size of the Largest Clone
*
F
Shannon Entropy
Melanocytes
Cancerized Field
Cancer Precursor Zone
Tumor
G
mCherry Skin
Cancerized Field
Cancer Precursor Zone
Small Patch
Tumor
log fraction nonresponding
1/13345
1/1236
1/806
1/378
1/348
dose (number of cells)

PLAsCAN (ANR-17-CONV-0002; J.C., S.D.), Institut National contre le Cancer (INCA-DGOS PRTK; J.C., S.D.), and Société Française de Dermatologie (SFD; J.C., S.D). This work was supported in part by the Office of the Assistant Secretary of Defense for Health Affairs (W81XWH-21-MRP-DA) and the Merchant Charitable Foundation. Y.C.K. is supported by a UQ Graduate School Scholarships (UQGSS) and Research Training Program (RTP) funded by the Australian Government, K.J.L. is supported by a National Health and Medical Research Council (NHMRC) Postgraduate Research Scholarship (GIN2013961) and a RTP scholarship. M.S.S. is supported by an NHMRC Investigator Award (2033440).

Figure 2

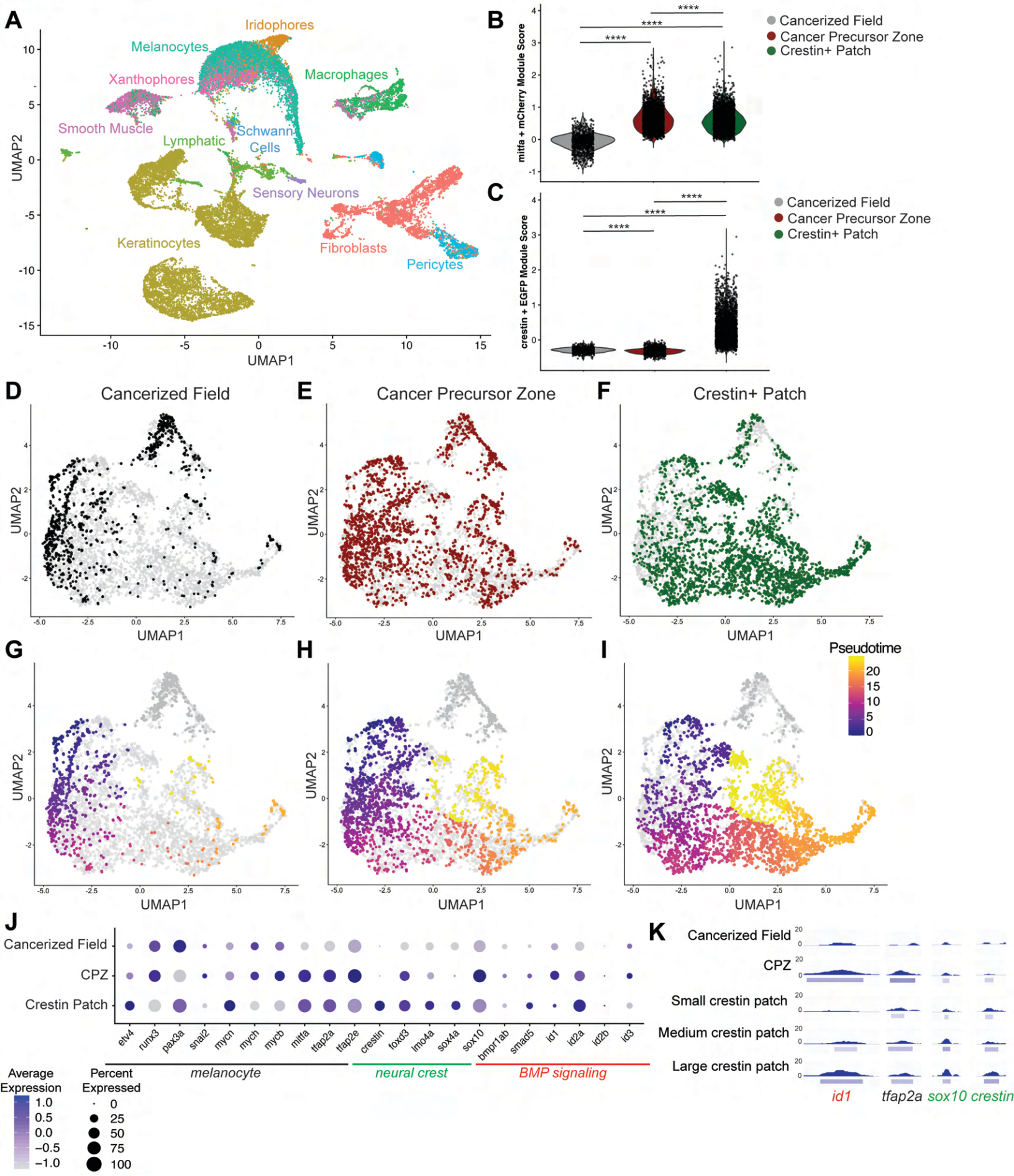
A
Iridophores
Melanocytes
Xanthophores
Macrophages
Smooth Muscle
Schwann Cells
Lymphatic
Sensory Neurons
Keratinocytes
Fibroblasts
Pericytes
UMAP1
UMAP2
B
mitfa + mCherry Module Score
Cancerized Field
Cancer Precursor Zone
Crestin+ Patch
C
crestin + EGFP Module Score
D
Cancerized Field
E
Cancer Precursor Zone
F
Crestin+ Patch
G
H
I
Pseudotime
J
Cancerized Field
CPZ
Crestin Patch
etv4
runx3
pax3a
snai2
mycn
mych
mycb
mitfa
tfap2a
tfap2e
crestin
foxd3
lmo4a
sox4a
sox10
bmpr1ab
smad5
id1
id2a
id2b
id3
melanocyte
neural crest
BMP signaling
Average Expression
Percent Expressed
K
Cancerized Field
CPZ
Small crestin patch
Medium crestin patch
Large crestin patch
id1
tfap2a
sox10
crestin

411 **Figure 2 | Single cell expression atlas of melanoma initiation. A**, UMAP of the
412 melanoma initiation atlas resulting from cancerized field (n=2) , CPZ (n=4), and patch
413 (n=2)-bearing zebrafish. **B, C.** Violin plot highlighting module enrichment for mitfa and
414 mCherry expression (**B**) or crestin and EGFP expression (**C**) for each cell within the
415 cancerized field, CPZ, or crestin+ stage. **D-F,** UMAP highlighting individual melanoma
416 stages for cancerized field (**D**), CPZ (**E**), and crestin+ (**F**) melanocytes. **G-I,** UMAP of
417 Pseudotime analysis with cancerized field melanocytes set as the root in cancerized
418 field (**G**), CPZ (**H**), and crestin+ (**I**) melanocytes. Dark gray cells are disconnected from
419 the main trajectory. **J**, Differentially expressed genes categorized into melanocyte
420 (black), neural crest (green), and BMP signaling (red). **K**, Open chromatin peaks in
421 promoter or enhancer regions of stage-specific genes.
422
423
424
425
426
427
428
429
430
431
432

Figure 3

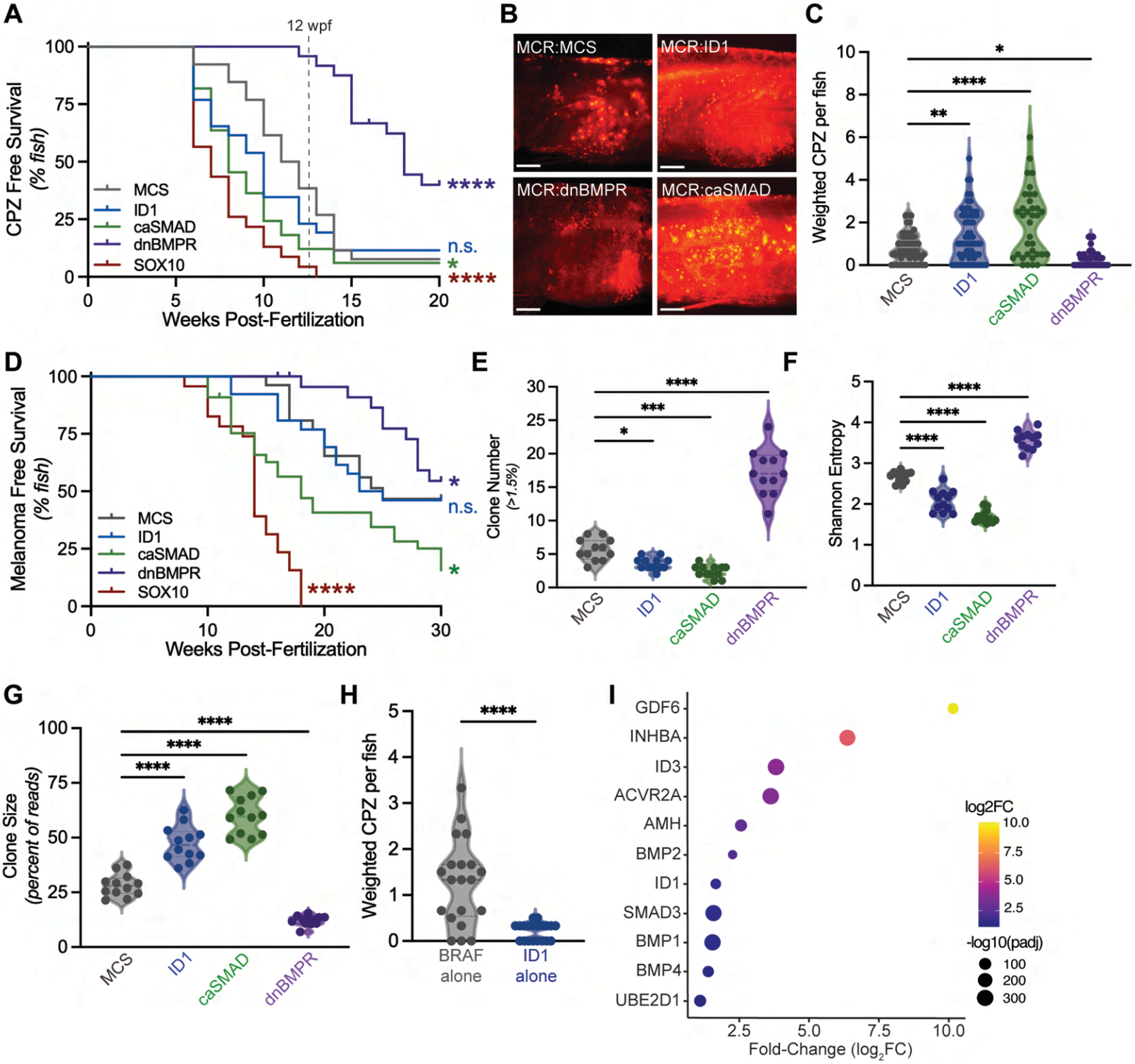
A
12 wpf
CPZ Free Survival (% fish)
Weeks Post-Fertilization
MCS
ID1
caSMAD
dnBMPR
SOX10
****
n.s.
*
****
B
MCR:MCS
MCR:ID1
MCR:dnBMPR
MCR:caSMAD
C
Weighted CPZ per fish
MCS
ID1
caSMAD
dnBMPR
D
Melanoma Free Survival (% fish)
Weeks Post-Fertilization
E
Clone Number (>1.5%)
F
Shannon Entropy
G
Clone Size (percent of reads)
H
Weighted CPZ per fish
BRAF alone
ID1 alone
I
GDF6
INHBA
ID3
ACVR2A
AMH
BMP2
ID1
SMAD3
BMP1
BMP4
UBE2D1
log2FC
-log10(padj)
Fold-Change (log2FC)

433 **Figure 3 | ID1 induces cancer precursor zone formation. A,** Kaplan-Meier curve of
434 CPZ incidence following modulation of the BMP pathway compared to MCS (control)
435 and SOX10 (known accelerator). n.s. = not significant; *p≤0.05; ****p≤0.0001; n>15. **B**,
436 Images showing *mitfa:mCherry* fluorescence in zebrafish overexpressing ID1, caSMAD,
437 or dnBMPR compared to an empty MCS control (12 wpf). **B**, Violin plot showing the
438 weighted number of cancer precursor zones per fish. Each dot represents one fish. * $p \leq$
439 0.05; ** $p \leq 0.01$; **** $p \leq 0.0001$. **D,** Kaplan-Meier curve of tumor incidence following
440 modulation of the BMP pathway compared to MCS (control) and SOX10 (known
441 accelerator). n.s. = not significant; *p≤0.05; ****p≤0.0001; n>15. **E-G,** Violin plot of the
442 total clone number with a minimum clone size of 1.5% (**E**), Shannon entropy (**F**), and
443 the largest clone as measured by the clone with the largest percent of total reads (**G**) in
444 a cohort of GESTALT barcoded fish (n=12 fish). *, p≤0.05; ****p≤0.0001. **H,** Violin plot
445 showing the weighted number of cancer precursor zones per fish in MCR:BRAF^{V600E}
446 relative to MCR:ID1 in wild type fish. Each dot represents one fish. ****p≤0.0001. **I,** Dot
447 plot of enriched BMP marker genes in PMEL(BRAFV600E) human cells relative to
448 PMEL without BRAF(V600E).
449
450
451
452
453
454
455

Figure 4

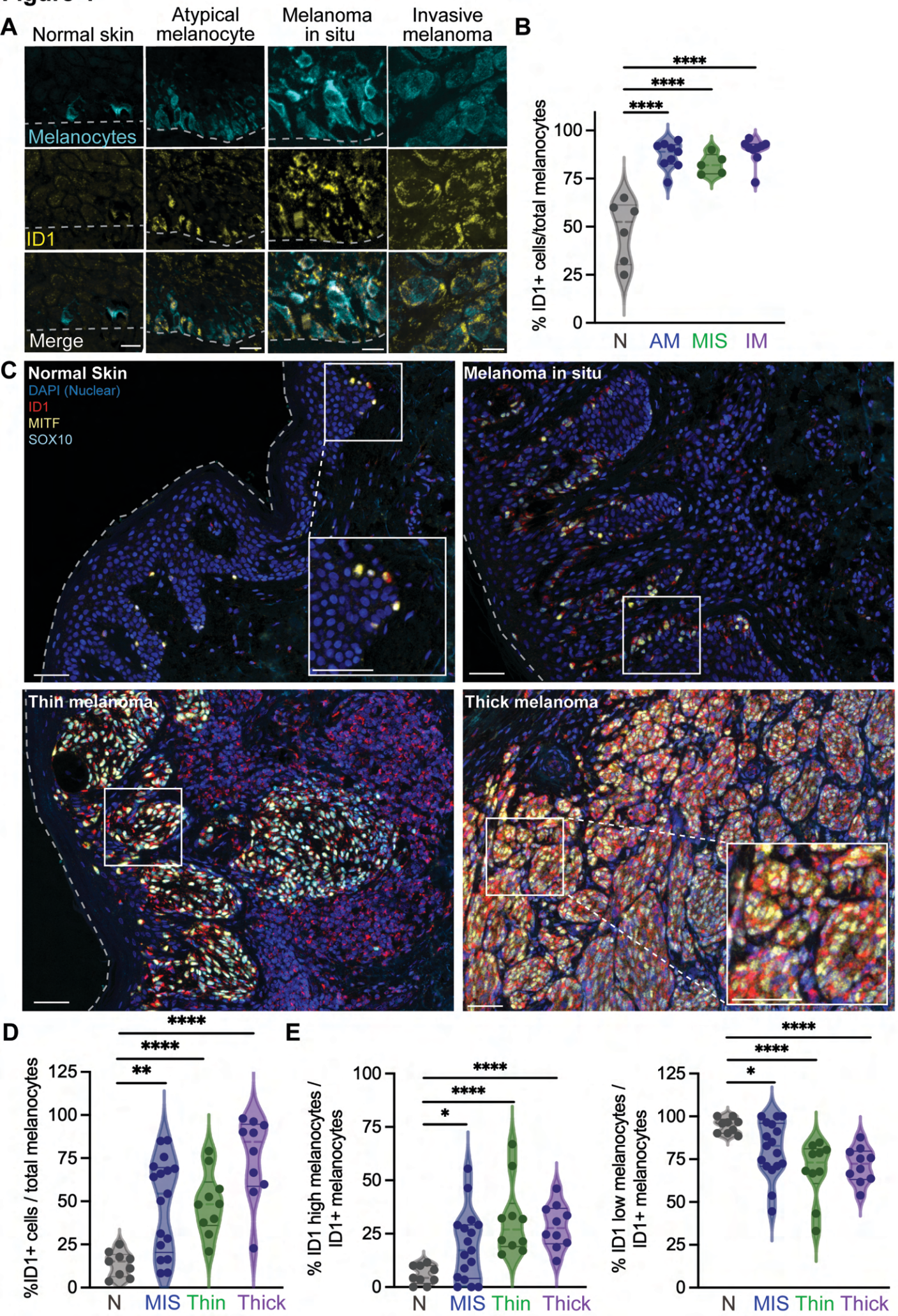
A
Normal skin
Atypical melanocyte
Melanoma in situ
Invasive melanoma
Melanocytes
ID1
Merge
B
% ID1+ cells/total melanocytes
N
AM
MIS
IM
C
Normal Skin
DAPI (Nuclear)
ID1
MITF
SOX10
Melanoma in situ
Thin melanoma
Thick melanoma
D
%ID1+ cells / total melanocytes
N
MIS
Thin
Thick
E
% ID1 high melanocytes / ID1+ melanocytes
% ID1 low melanocytes / ID1+ melanocytes

456 **Figure 4 | ID1 is upregulated during human melanoma initiation and progression.**
457 **A,** Immunofluorescent staining of melanocytes (MART1) and ID1 in human skin
458 samples. Scale bars, 10 μm. **B**, Percent of melanocytes that are positive for ID1. Each
459 dot represents one patient (n =5-9). **p≤0.01; ****p≤0.0001. **C**, Immunofluorescent
460 staining of melanocytes (SOX10 or MITF, yellow), ID1 (red), and DAPI (blue) in human
461 skin and melanoma samples. Inset highlights regions of double positive melanocytes
462 (MITF/SOX10^{+}; ID1^{+}). Scale bars, 50 μm. **D,** Percent of melanocytes that are positive
463 for ID1. Each dot represents one patient (n = 9-17). **p≤0.01; ****p≤0.0001. **E,** Percent
464 of melanocytes that are positive for ID1 with high ID1 expression (left) or low ID1
465 expression (right) across melanoma stages. Each dot represents one patient (n = 9-17).
466 p≤0.05; **p≤0.01; ****p≤0.0001.
467
468
469
470
471
472
473
474
475
476
477

Figure 5

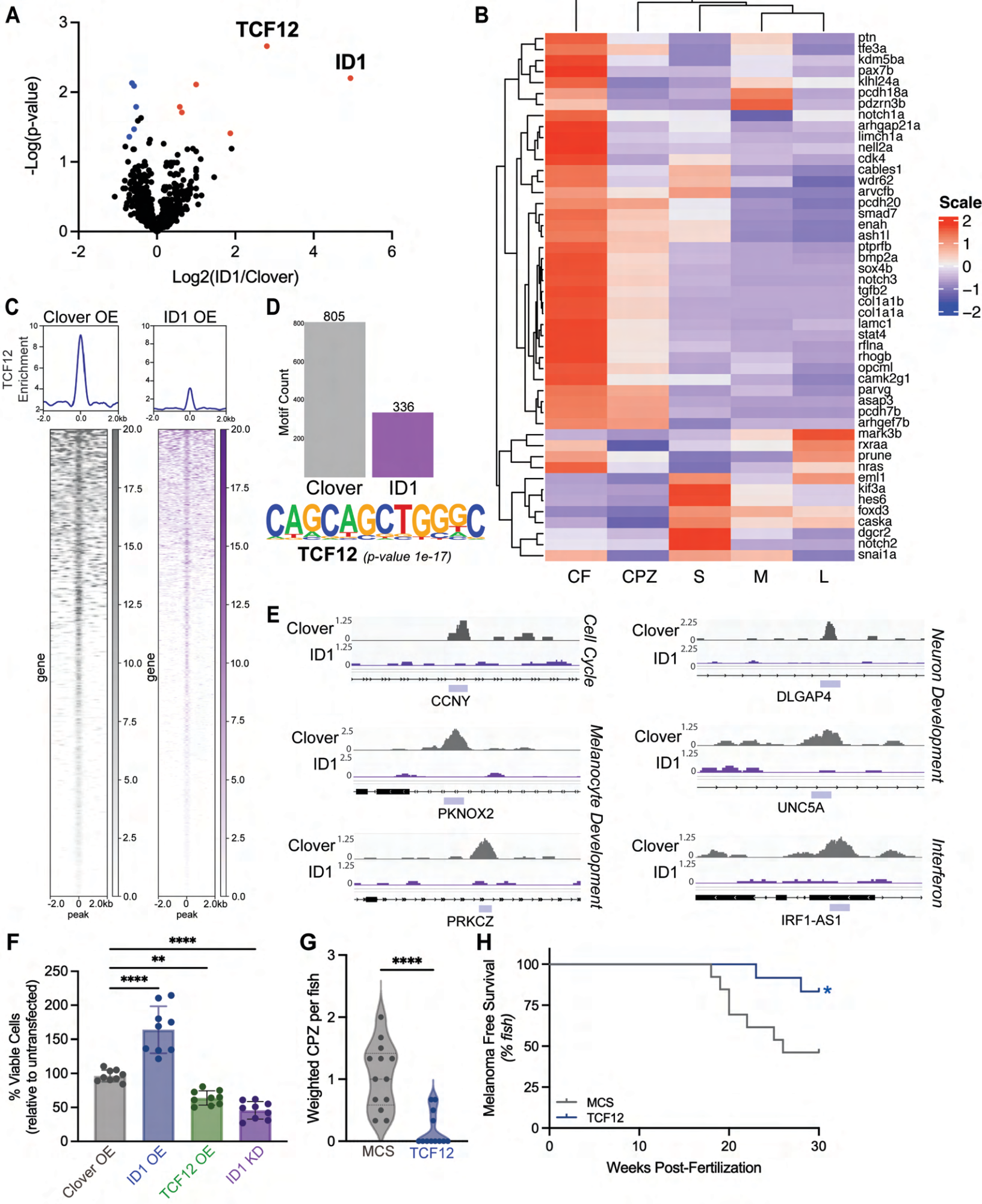
A
TCF12
ID1
-Log(p-value)
Log2(ID1/Clover)
B
Scale
CF
CPZ
S
M
L
C
Clover OE
ID1 OE
TCF12 Enrichment
gene
peak
D
805
336
Motif Count
Clover
ID1
TCF12 (p-value 1e-17)
E
Clover
ID1
CCNY
Cell Cycle
DLGAP4
Neuron Development
PKNOX2
Melanocyte Development
UNC5A
PRKCZ
IRF1-AS1
Interferon
F
% Viable Cells (relative to untransfected)
Clover OE
ID1 OE
TCF12 OE
ID1 KD
G
Weighted CPZ per fish
MCS
TCF12
H
Melanoma Free Survival (% fish)
MCS
TCF12
Weeks Post-Fertilization

Figure 5 | ID1 sequesters TCF12 from chromatin to drive cancer precursor zone formation through loss of development and signaling regulatory genes. A, Volcano plot analysis of IP-MS data comparing proteins bound to ID1 vs Clover pull down. **B**, Heatmap of TCF12 targets identified by their decreased expression in the context of ID1 overexpression and the presence of a TCF12 motif in the promoter/enhancer region. **C,** Heatmaps depicting ChIP-seq peak structure following Clover (left, gray) or ID1 (right, purple) overexpression in PMEL($BRAF^{V600E}$) cells. A kb window is centered on the peak center highlighting peaks lost after ID1 overexpression. **D,** Quantification of peaks with TCF12 motifs following Clover (n=805) or ID1 (n=336) overexpression. TCF12 motif is only enriched in Clover overexpressing cells (p = 1e-17). **E,** IGV tracks of TCF12 motif containing peaks in clover (gray) or ID1 (purple) overexpressing cells. Purple bar indicates peak called by MACS. **F,** Bar graph representing viable cells relative to non-transfected controls following Clover, ID1, or TCF12 overexpression or ID1 knockdown in PMEL($BRAF^{V600E}$) ***p≤0.01; ****p≤0.001. **G,** Violin plot showing the weighted number of cancer precursor zones following TCF12 overexpression relative to empty control. Each dot represents one fish; n=12. ****p≤0.001. **H,** Kaplan-Meier curve of melanoma incidence. Melanoma incidence is delayed in TCF12 overexpressing fish that develop CPZs. *p≤0.05, n=12.